

Article

High Performance of Manganese Porphyrin Sensitized p-Type CuFe_2O_4 Photocathode for Solar Water Splitting to Produce Hydrogen in a Tandem Photoelectrochemical Cell

Xia Li ¹, Aijuan Liu ¹, Dongmei Chu ¹, Chunyong Zhang ¹, Yukou Du ¹ , Jie Huang ² and Ping Yang ^{1,*} 

¹ College of Chemistry, Chemical Engineering and Materials Science, Soochow University, Suzhou 215123, China; lixia1011@163.com (X.L.); liuajiansuda@163.com (A.L.); dmchu2015@126.com (D.C.); zhangchunyong@126.com (C.Z.); duyk@suda.edu.cn (Y.D.)

² Key Laboratory of Nano-Bio Interface, Division of Nanobiomedicine, Suzhou Institute of Nano-Tech and Nano-Bionics, Chinese Academy of Sciences, Suzhou 215123, China; jhuang2008@sinano.ac.cn

* Correspondence: pyang@suda.edu.cn; Tel.: +86-512-6588-0089

Received: 22 January 2018; Accepted: 6 March 2018; Published: 9 March 2018

Abstract: A novel composite composed of (5, 10, 15, 20-tetraphenyl) porphyrinato manganese sensitized p-type CuFe_2O_4 was developed for constructing the photocathode of a tandem photoelectrochemical (PEC) cell. The prepared material was characterized by X-ray diffraction (XRD), transmission electron microscopy (TEM), X-ray photoelectron spectroscopy (XPS) and UV-vis diffuse reflectance spectroscopy (DRS). Light-driven water splitting to produce hydrogen can be achieved through the PEC cell, and the results show that H_2 and O_2 can be collected separately at low applied bias. This work demonstrates that manganese porphyrin sensitized CuFe_2O_4 is an effective hybrid material for building the photocathode of a PEC cell for solar water splitting to produce H_2 .

Keywords: CuFe_2O_4 ; nanocomposite photocathode; photoelectrochemical cell; water splitting; hydrogen production

1. Introduction

In recent years, hydrogen, acting as an environmentally friendly energy carrier with high capacity, has attracted great attention owing to increasing environmental concerns and energy demands. Photocatalytic water splitting to produce hydrogen can be regarded as one of the most promising strategies for converting solar energy into chemical fuels [1,2]. Over the past decades, much effort has been devoted to exploring new materials for fabricating electrodes for photoelectrochemical (PEC) cells [3,4]. In general, a PEC cell is constructed by an anode and a cathode, from which oxygen and hydrogen can be produced and collected. The photocathode is usually composed of a p-type semiconductor with suitable bandgap. Under sunlight illumination, the electrons in the valence band of the p-type photocatalyst are excited to its conduction band. If the potential of the photoexcited electrons accumulated on the conduction band is high enough to be able to overcome the surface potential and migrate to the interface of the electrode and electrolyte, they can act as a reducing agent to reduce water into hydrogen. So far, a large number of p-type semiconductors, including Cu_2O or CuO [5–7], NiO [8,9], InP [10,11], etc., have been reported as photocathode materials for light-driven water splitting [12–16]. Among them, Cu_2O has received the most attention, with favorable CB edge position and direct band gap; however, it is unstable in aqueous solutions under illumination [17]. CuFe_2O_4 as a spinel ferrite has been regarded as a promising catalyst for photocatalytic H_2 production owing to the relatively narrow band gap, low cost and photochemical stability [18,19]. Although

the photocurrent of CuFe_2O_4 is relatively modest compared to that of Cu_2O , its onset potential is at a lower level, which is beneficial for photocatalysis [20].

Porphyrin-based dyes have been known to be used as potential sensitizers, owing to their high extinction coefficients in the visible light region, excellent chemical and thermal stability, efficient photochemical electron transfer ability, and low cost [21–23]. Porphyrin dye-modified semiconductor electrodes can improve the photophysical and electronic properties of PEC cells greatly [24].

In this study, we report a p-type CuFe_2O_4 -based photocathode sensitized with (5, 10, 15, 20-tetraphenyl) porphinato manganese(III) (MnTPP). MnTPP acts as a light-harvesting photosensitizer and broadens the range of light absorption of photocathode. MnTPP modified CuFe_2O_4 electrode displays a remarkable enhanced photoelectrochemical water splitting performance.

2. Results

2.1. Morphology and Structure

XRD patterns of the samples are shown in Figure 1A. Six diffraction peaks at 30.1° , 35.4° , 43.2° , 50.4° , 62.5° , and 74.1° correspond to (220), (311), (400), (107), (440), and (533) planes of the cubic spinel structure of CuFe_2O_4 (JCPDS card no. 25–0283). In addition, the relatively regular diffraction peaks without the peaks of other impurities show the high purity of CuFe_2O_4 . The diffraction peaks of MnTPP/ CuFe_2O_4 match well to those of pure CuFe_2O_4 , indicating that the presence of MnTPP in the hybrid does not change the crystallinity of CuFe_2O_4 . The TEM image of the CuFe_2O_4 sample (Figure 1B) shows that the as-prepared CuFe_2O_4 sample is composed of nanospheres with a rough surface. The average diameter of the nanospheres is 50–60 nm.

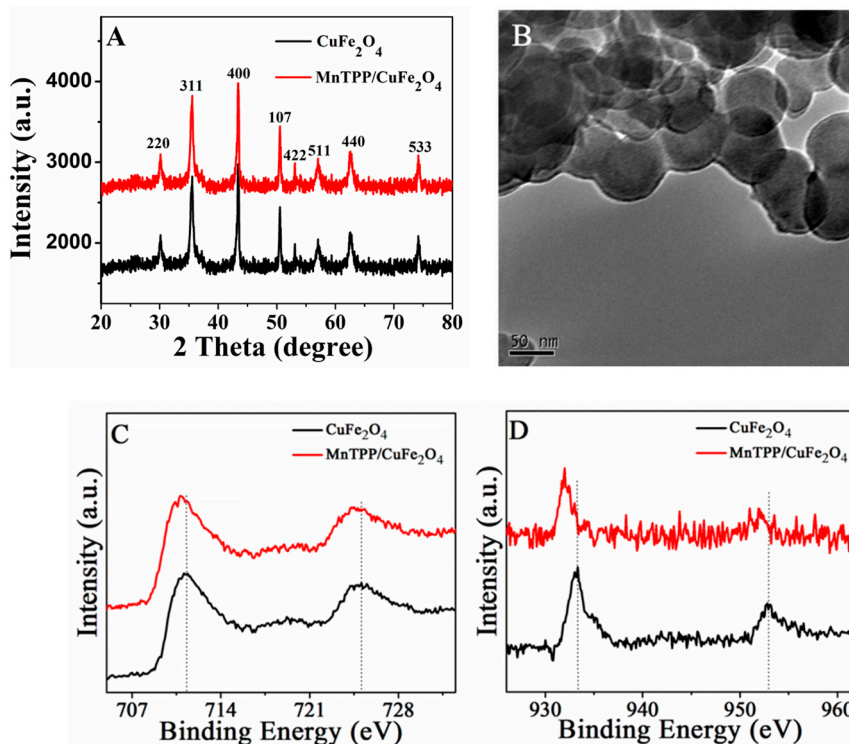


Figure 1. (A) XRD patterns of CuFe_2O_4 and MnTPP/ CuFe_2O_4 ; (B) TEM image of CuFe_2O_4 ; high-resolution XPS spectra of (C) Fe 2p and (D) Cu 2p of CuFe_2O_4 .

The Fe 2p XPS spectrum of CuFe_2O_4 (Figure 1C) shows two dominant peaks with binding energies of Fe $2p_{3/2}$ and Fe $2p_{1/2}$ at 711.3 and 725.1 eV along with a typical satellite peak at 718.6 eV, suggesting the presence of Fe^{3+} in the sample [25]. Each Fe 2p lines can be deconvoluted into two peaks, as shown

in Figure S1A. The doublets of Fe 2p_{3/2} binding energy at 710.4 eV and Fe 2p_{1/2} binding energy at 723.7 eV are assigned to the Fe³⁺ ions in octahedral sites, while the doublets of Fe 2p_{3/2} binding energy at 712.8 eV and Fe 2p_{1/2} binding energy at 725.7 eV are assigned to Fe³⁺ ions in tetrahedral sites [26]. Moreover, the relative contributions to the overall intensity of Fe³⁺ ions at the octahedral and tetrahedral sites are 40% and 60%, calculated from the ratio of peak area. The Cu 2p spectrum of CuFe₂O₄ (Figure 1D) shows two main peaks located at 933.2 and 952.8 eV, corresponding to the Cu 2p_{3/2} and Cu 2p_{1/2} of Cu²⁺, respectively [20]. Along with a typical satellite peak at 942.8 eV, the above result indicates the presence of Cu²⁺ in synthesized CuFe₂O₄. Moreover, each Cu 2p peak can also be fitted to two peaks, as shown in Figure S1B. The doublets of Cu 2p_{3/2} binding energy at 933.2 eV and Cu 2p_{1/2} binding energy at 952.8 eV are assigned to the Cu²⁺ ions in octahedral sites, while the doublets of Cu 2p_{3/2} binding energy at 935.1 eV and Cu 2p_{1/2} binding energy at 955.0 eV are assigned to the Cu²⁺ ions in tetrahedral sites. The relative contributions to the overall intensity of Cu²⁺ ions at the octahedral and tetrahedral sites are 51% and 49%, respectively [27]. These results are consistent with that of the CuFe₂O₄ nanospheres prepared by the reported hydrothermal method [28]. The Cu 2p peaks' intensity and the width of the MnTPP/CuFe₂O₄ showed a decrease compared to CuFe₂O₄, which may attributed to a decrease of the content and the number of inequivalent sites of Cu on the composite's surface when increasing the MnTPP ratio in the composite [29,30]. In addition, a negative shift or a smaller peak binding energy is observed for both Fe 2p and Cu 2p peaks in the XPS spectra of the MnTPP/CuFe₂O₄ sample, this result shows the formation of new chemical bonds after combining MnTPP with CuFe₂O₄, demonstrating that there is an interaction between MnTPP and CuFe₂O₄ in the nanohybrid [31]. The XPS spectra of Mn 2p in the MnTPP/CuFe₂O₄ material (Figure S1C) exhibits two peaks centered on 642.4 and 654.5 eV, corresponding to Mn 2p_{3/2} and Mn 2p_{1/2}, respectively. The above results provide an evidence that the MnTPP-modified CuFe₂O₄ hybrid had been successfully synthesized.

2.2. Optical and Photoelectrochemical Properties

Figure 2 displays the UV-vis diffuse reflectance spectra of the prepared samples. From the figure, we can see that CuFe₂O₄ demonstrates a wide light absorption throughout the whole UV-vis region, which is in agreement with previous reports [32,33], and the MnTPP dye exhibits a strong Soret band at 455 nm and two weak Q bands at 570 and 610 nm, respectively [34]. The spectrum of the MnTPP/CuFe₂O₄ composite exhibits broad absorption ability in visible light region, with the characteristic absorption of MnTPP bands centered at 464 and 614 nm. These facts demonstrate that the MnTPP/CuFe₂O₄ composite has an enhanced ability to harvest visible light, as compared to bare CuFe₂O₄. The Tauc plot (inset of Figure 2) shows that the band gap is 1.42 eV for CuFe₂O₄ in the hybrid structure, which is in agreement with the value given in previous reports [35,36].

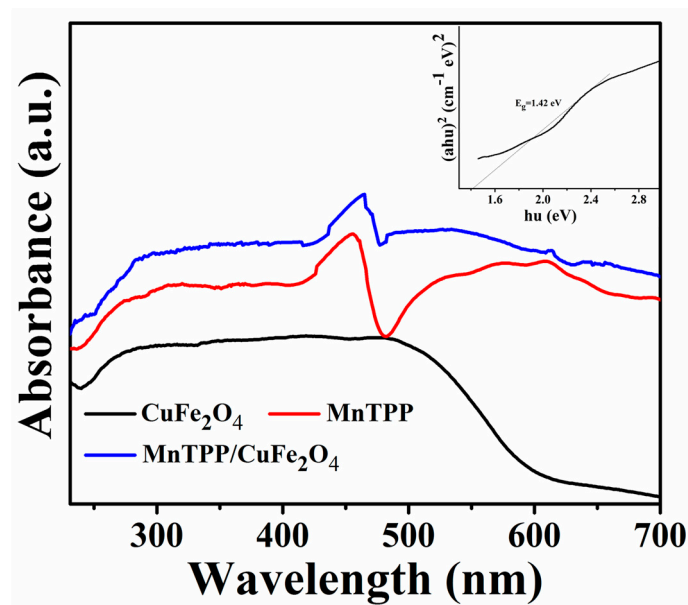


Figure 2. DRS spectra of the samples. Inset: the plots of $(\alpha h\nu)^2$ vs. energy $h\nu$ for CuFe_2O_4 .

The linear scan voltammograms of CuFe_2O_4 are shown in Figure 3A. It is obvious that the cathodic current of CuFe_2O_4 under illumination is larger than the dark current, which is characteristic of a p-type semiconductor [37,38]. The fact that dark current of the fabricated photocathode is a bit high may be due to the existing surface states on the photocathode materials, resulting in the leakage current [39,40]. The negative slope of the Mott-Schottky curve of CuFe_2O_4 (Figure 3B) further proves that p-type CuFe_2O_4 semiconductor has been successfully fabricated, and the calculated flat-band potential of CuFe_2O_4 is 0.14 V vs. RHE, which can be approximately considered to be the valence band value for p-type semiconductors. Combined with the value of the band gap (1.42 eV), we can conclude that the conduction band edge of CuFe_2O_4 is -1.28 V vs. RHE. The photoelectrochemical results of the prepared samples are shown in Figure 3C. The $\text{CuFe}_2\text{O}_4/\text{ITO}$ electrode shows a weak photocurrent density ($-0.04 \mu\text{A cm}^{-2}$) under UV-vis light irradiation; whereas the observed photocurrent density of the MnTPP/ITO electrode is $-0.11 \mu\text{A cm}^{-2}$ in the same conditions, which can be caused by the strong optical absorption of MnTPP and effective photoexcited electron transfer from the sensitizer to FTO. Compared with the photocurrent of CuFe_2O_4 and MnTPP , the $\text{MnTPP}/\text{CuFe}_2\text{O}_4/\text{FTO}$ electrode demonstrates a remarkably enhanced photocurrent density ($-0.34 \mu\text{A cm}^{-2}$), owing to broad and strong absorption of the MnTPP moiety and efficient electron transfer from the excited dye to CuFe_2O_4 , resulting in effective photoexcited charge separation [41]. The electrochemical impedance spectra (EIS) of CuFe_2O_4 electrode and $\text{MnTPP}/\text{CuFe}_2\text{O}_4$ electrode are shown in Figure 3D. The radius of the $\text{MnTPP}/\text{CuFe}_2\text{O}_4$ plot is smaller than that of CuFe_2O_4 , indicating a smaller resistance and an improvement of charge transfer on the interface between $\text{MnTPP}/\text{CuFe}_2\text{O}_4$ and the electrolyte [22,42].

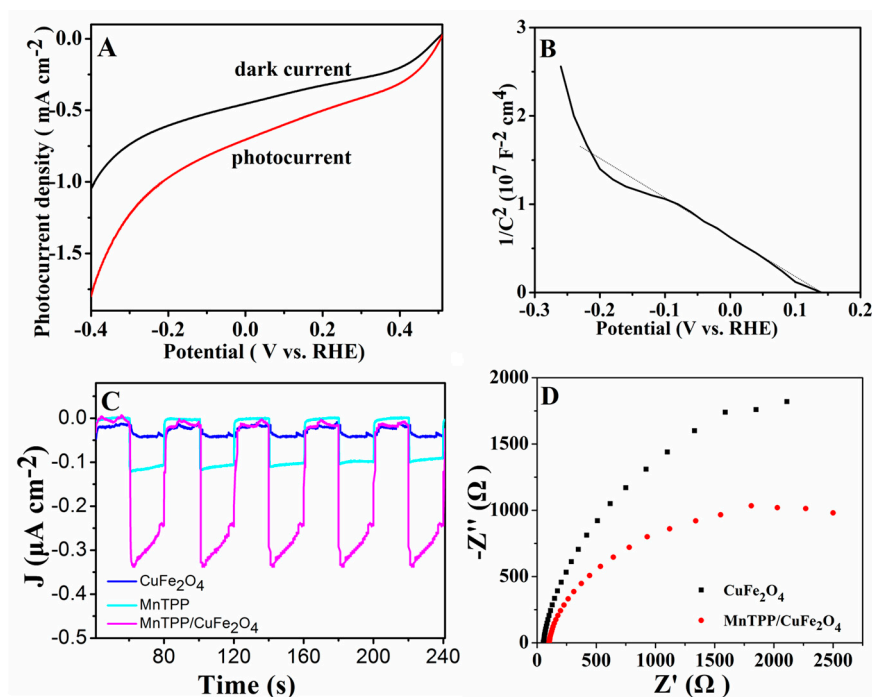


Figure 3. (A) Linear sweep voltammograms of CuFe_2O_4 ; (B) Mott-Schottky plot of CuFe_2O_4 ; (C) Photocurrent responses of CuFe_2O_4 , MnTPP and MnTPP/ CuFe_2O_4 recorded at -0.2 V vs. SCE; (D) Nyquist plots of (EIS) for samples. The electrodes were impregnated in 0.2 M Na_2SO_4 solution (pH ~ 6) and illuminated by a 150 W xenon lamp.

2.3. Photocatalytic Activity

For all photocatalytic experiments carried out in the tandem PEC cell, the molar amount of O_2 detected from the counter electrode is about $1/2$ of that of H_2 . Figure S2 shows the amount of hydrogen collected from photocathode under -0.2 V applied bias vs. RHE. In 2 h irradiation of a solar simulator (Ultra-vitalux, 300 W, Osram, Augsburg, Germany), the amount of hydrogen collected from the CuFe_2O_4 chamber is $11.1 \mu\text{mol g}^{-1}$. Under the same conditions, the amount of hydrogen collected from the MnTPP/ CuFe_2O_4 chamber reaches $23.0 \mu\text{mol g}^{-1}$, indicating a positive photocatalytic influence of the combination of MnTPP and CuFe_2O_4 . Platinizing the electrode can further strengthen the activity of the dye-sensitized electrode. The amount of hydrogen evolved from the Pt/MnTPP/ CuFe_2O_4 electrode after 2 h of reaction increases to $760.0 \mu\text{mol g}^{-1}$ under -0.2 V vs. RHE bias. For comparison, we used a Pt plate to replace the prepared photocathode. Neither hydrogen nor oxygen can be detected from the tandem PEC cell under the same reaction conditions. Figure 4 and the inset of Figure 4 show that hydrogen can also be collected from CuFe_2O_4 ($9.3 \mu\text{mol g}^{-1}$), MnTPP/ CuFe_2O_4 ($12.0 \mu\text{mol g}^{-1}$), and Pt/MnTPP/ CuFe_2O_4 ($748.0 \mu\text{mol g}^{-1}$) electrode under -0.1 V applied bias vs. RHE, respectively, indicating that as-prepared photocathodes still have catalytic activity at very low applied bias. The Faraday efficiency for H_2 production and solar-to-hydrogen conversion efficiency η_{STH} from Pt/MnTPP/ CuFe_2O_4 PEC cell at -0.1 V vs. RHE are 53% and 0.14%, respectively.

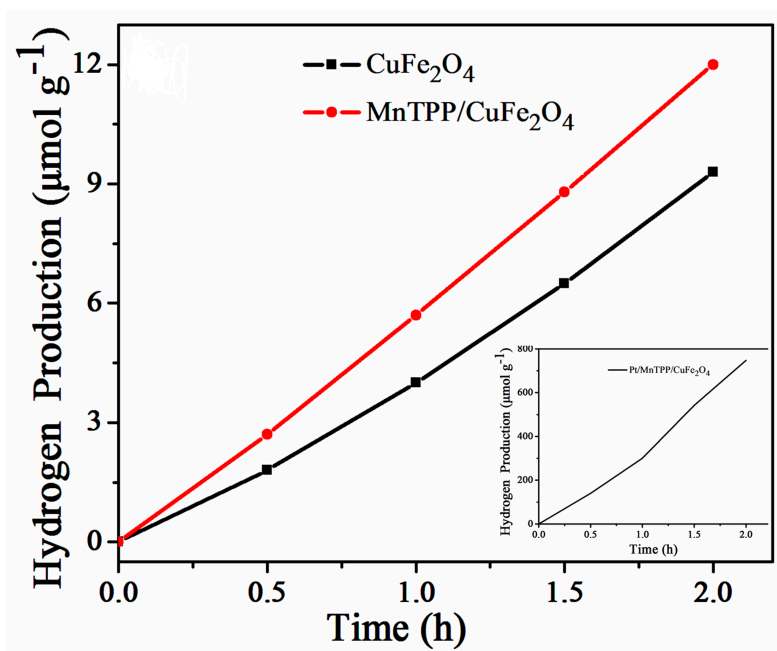


Figure 4. Amount of hydrogen evolved from the PEC device with the samples at -0.1 V. Inset shows the amount of H_2 evolved over Pt/MnTPP/CuFe₂O₄. Reaction conditions: 0.2 M phosphate buffer solution. Light intensity: 16 mW cm^{-2} .

The incident photon-to-electron conversion efficiency (IPCE) spectrum of MnTPP/CuFe₂O₄ electrode (Figure S3) shows a maximum IPCE of 22.8% at 475 nm and 22.7% at 585 nm. This result fits well the UV-visible diffuse reflectance spectra of MnTPP/CuFe₂O₄. Figure S4A–C shows the results of the photocurrent experiments of the as-prepared photocathodes. The steady-state photocurrent changes in the order: Pt/MnTPP/CuFe₂O₄ > MnTPP/CuFe₂O₄ > CuFe₂O₄, which is consistent with the amount of hydrogen evolved from the PEC cell. The photocurrent of the Pt/MnTPP/CuFe₂O₄ electrode remains constant from the very beginning to 6 h of continuous operation at the -0.1 V and -0.2 V bias, indicating sufficient stability for the photocatalysis.

3. Materials and Methods

3.1. Materials

Cupric chloride (CuCl₂·2H₂O), ferric chloride (FeCl₃·6H₂O), acetic acid (NaAc), polyvinylpyrrolidone (PVP) disodium hydrogen phosphate (Na₂HPO₄), sodium dihydrogen phosphate (NaH₂PO₄), (hydro)chloroplatinic acid (H₂PtCl₆) and (5, 10, 15, 20-tetraphenyl) porphinato manganese (MnTPP) were obtained from Sinopharm Chemicals Reagent Co., Ltd, Shanghai, China. Double distilled water was used throughout the experiments. 0.2 M phosphate buffer solution was chosen to be the electrolyte. All the reagents were used without other purification.

3.2. Photoelectrode Preparation

CuFe₂O₄ nanospheres were prepared by a hydrothermal method [28]. In a typical synthesis, 2 mmol of CuCl₂·2H₂O, 4 mmol of FeCl₃·6H₂O, 6 mmol of NaAc and 0.5 g of polyvinylpyrrolidone (PVP) were dissolved into 30 mL of ethylene glycol, and stirred at room temperature for 30 min. Then the mixture was transferred into an 80 mL Teflon-lined autoclave and maintained at 160 °C for 24 h. The solid was achieved from the mixture through centrifugation, and washed with deionized water three times. Finally, the solid was dried at 60 °C under vacuum. For fabricating the CuFe₂O₄ photoelectrode, a CuFe₂O₄ suspension was prepared by adding and grinding the CuFe₂O₄ powder (20

mg) with a solution composed by 3 mL of trichloromethane, ethylene glycol, ethanol, and PVP (10 mL: 15 mL: 75 mL: 30 mg). CuFe₂O₄ was deposited by doctor blading the suspension on a clean FTO glass (6 cm in diameter). The electrode was dried at 60 °C, after that it was calcined under 400 °C for 2 h in air. The obtained electrode was dipped in MnTPP ethanol solution (1 mg mL⁻¹) for 2 h and then was dried at 60 °C to get MnTPP-sensitized CuFe₂O₄ electrode (MnTPP/CuFe₂O₄). The MnTPP/CuFe₂O₄ electrode was impregnated in 0.1 mM H₂PtCl₆ solution and illuminated by a 150 W xenon lamp at room temperature for 1 h, resulting in platinized modified MnTPP/CuFe₂O₄ electrode.

3.3. Characterization

Transmission electron microscopy (TEM) studies were carried out on a FEI TECNAI-G2 electron F20 200 KV microscope (JEOL JEM-2100, JEOL Ltd., Tokyo, Japan). The X-ray diffraction (XRD) patterns were measured on X'Pert-Pro MRD (Amsterdam, The Netherlands) equipped with Ni-filtered Cu K α radiation. X-ray photoelectron spectroscopy (XPS) measurement was carried out on ESCALAB 250 XI with an AXIS Ultra DLD system (Kratos Analytical Ltd., Manchester, UK). UV-vis diffuse reflectance absorption spectra (DRS) were carried out on a UV3600 spectrophotometer (Shimadzu, Kyoto, Japan). Photoelectrochemical measurements were performed on a CHI 660D potentiostat/galvanostat electrochemical analyzer (CHI Instrument, Inc., Shanghai, China) in a three-electrode system consisting of a working electrode, a saturated calomel electrode (SCE) and a platinum plate. The working electrode was prepared by dipping ca. 0.5 mL of the sample dispersion (0.4 mg mL⁻¹) on a clean fluorine-doped tin oxide (FTO) glass and drying under ambient conditions. The efficient area of the electrode was about 1.0 cm². Three electrodes were immersed in 0.2 M Na₂SO₄ (pH = 6), which acted as the electrolyte solution. The working electrode was irradiated by a GY-10 xenon lamp (150 W) as light source.

3.4. Photocatalytic Reaction

The photocatalytic reaction was performed in a three-electrode PEC device, as depicted in Scheme S1. The CuFe₂O₄ or MnTPP/CuFe₂O₄ photoelectrode acted as photocathode, a platinum plate as counter electrode and an SCE as the reference electrode. Three electrodes are connected through a potentiostat, and the system was deaerated by pumping argon into the system for 30 min before the reaction. The working electrode was illuminated by a solar simulator (Ultra-vitalux, 300 W) at 298 K. The distance between the lamp and the quartz window of the PEC cell was 20 cm. The gases produced from the reaction were analyzed by an online gas chromatograph (GC1690, Ke Xiao Instruments Co., Ltd., Hangzhou, China), which has a thermal conductivity detector and 5 Å molecular sieve columns; argon was used as carrier gas. GC signal calibration was performed by the standard H₂/Ar gas mixtures with known concentrations.

The apparent quantum yield (AQY) was studied by the solar simulator with a 420 nm filter acting as light source. The focused light intensity was measured on a radiometer. AQY is calculated by the Equation (1):

$$\text{AQY (\%)} = \frac{\text{number of reacted electrons}}{\text{number of incident photons}} \times 100 = \frac{2 \times n_{\text{H}_2}}{I_0 \times t} \times 100 \quad (1)$$

where n_{H_2} is the measured molar number of H₂ at the reaction t , and I_0 is the number of photons per unit time. I_0 there was ca. 4.5×10^{-8} mol s⁻¹.

Solar-to-hydrogen conversion efficiency η_{STH} from the PEC cell at -0.1 V vs. RHE is calculated by the following equation [43–45]:

$$\eta_{\text{STH}} = \frac{\{J_{\text{OP}} [\text{mA} \cdot \text{cm}^{-2}] \times (V - V_{\text{bias}}) \times \eta_{\text{F}}\}}{P_{\text{light}} [\text{mW} \cdot \text{cm}^{-2}]} \times 100 \quad (2)$$

where J_{op} is the effective operating current density measured during the reaction ($35.7 \mu\text{A cm}^{-2}$), V is the water splitting potential required (1.23 V), V_{bias} is the bias voltage between two electrodes, P_{light} is the incident light power (16 mW cm^{-2}), and η_F is the Faraday efficiency (55%).

4. Conclusions

In summary, we demonstrated a novel material composed of porphyrinato manganese sensitized p-type CuFe_2O_4 , which has been successfully applied to fabricate a photocathode for water splitting to produce hydrogen. The gases produced from the PEC cell can be collected separately at very low bias. This study provides a new approach to obtaining both practical and reliable materials for photocatalytic applications.

Supplementary Materials: The following are available online at <http://www.mdpi.com/2073-4344/8/3/108/s1>, Figure S1: High-resolution XPS spectra of (A) Fe 2p and (B) Cu 2p of CuFe_2O_4 nanospheres; (C) Mn 2p from MnTPP/ CuFe_2O_4 hybrid. Figure S2: Amount of hydrogen evolved from the PEC device with CuFe_2O_4 , MnTPP/ CuFe_2O_4 and Pt/MnTPP/ CuFe_2O_4 at -0.2 V applied bias vs. RHE. Reaction conditions: electrolyte 0.2 M phosphate buffer solution. Light intensity 16 mW cm^2 . Figure S3: IPCE spectra of the PECs in 0.2 M phosphate buffer solution without any bias voltage. Figure S4: Current density vs. time behavior from the PEC device with (A) CuFe_2O_4 ; (B) MnTPP/ CuFe_2O_4 and (C) Pt/MnTPP/ CuFe_2O_4 as the photocathode at different applied voltages vs. RHE. Reaction conditions: electrolyte 0.2 M phosphate buffer solution. Light intensity 16 mW cm^2 . Scheme S1: Scheme of three-electrode PEC device. Table S1: comparison of the performance of photocathodes.

Acknowledgments: The authors are grateful for the financial support of this research by the National Natural Science Foundation of China (21373143), The Priority Academic Program Development of Jiangsu Higher Education Institutions (PAPD) and the project of scientific and technologic infrastructure of Suzhou (SZS201708).

Author Contributions: P.Y., Y.D. and J.H. conceived and designed the experiments; X.L., A.L., D.C., J.H. and C.Z. performed the experiments; X.L., P.Y. and J.H. analyzed the data and wrote the manuscript.

Conflicts of Interest: The authors declare no conflict of interest.

References

1. Zhang, W.; Lai, W.; Cao, R. Energy-related small molecule activation reactions: Oxygen reduction and hydrogen and oxygen evolution reactions catalyzed by porphyrin- and corrole-based systems. *Chem. Rev.* **2017**, *117*, 3717–3797. [[CrossRef](#)] [[PubMed](#)]
2. Wang, D.; Huang, J.; Li, X.; Yang, P.; Du, Y.; Goh, C.; Lu, C. Photocatalytic H_2 production under visible-light irradiation based on covalent attachment of manganese phthalocyanine to graphene. *J. Mater. Chem. A* **2015**, *3*, 4195–4202. [[CrossRef](#)]
3. Hao, C.; Wang, W.; Zhang, R.; Zou, B.; Shi, H. Enhanced photoelectrochemical water splitting with $\text{TiO}_2@Ag_2O$ nanowire arrays via p-n heterojunction formation. *Sol. Energy Mater. Sol. Cells* **2018**, *174*, 132–139. [[CrossRef](#)]
4. She, X.; Zhang, Z.; Baek, M.; Yong, K. Photoelectrochemical enhancement of $\text{ZnO}/\text{BiVO}_4/\text{ZnFe}_2\text{O}_4$ /rare earth oxide hetero-nanostructures. *Appl. Surf. Sci.* **2017**, *429*, 29–36. [[CrossRef](#)]
5. Masudy-Panah, S.; Moakhar, R.S.; Chua, C.S.; Tan, H.R.; Wong, T.I.; Chi, D.; Dalapati, G.K. Nanocrystal engineering of sputter-grown CuO photocathode for visible-light-driven electrochemical water splitting. *ACS Appl. Mater. Interfaces* **2016**, *8*, 1206–1213. [[CrossRef](#)] [[PubMed](#)]
6. Masudy-Panah, S.; Moakhar, R.S.; Chua, C.S.; Kushwaha, A.; Dalapati, G.K. Stable and efficient CuO based photocathode through oxygen-rich composition and Au-Pd nanostructure incorporation for solar-hydrogen production. *ACS Appl. Mater. Interfaces* **2017**, *9*, 27596–27606. [[CrossRef](#)] [[PubMed](#)]
7. Masudy-Panah, S.; Moakhar, R.S.; Chua, C.S.; Kushwaha, A.; Wong, T.I.; Dalapati, G.K. Rapid thermal annealing assisted stability and efficiency enhancement in a sputter deposited CuO photocathode. *RSC Adv.* **2016**, *6*, 29383–29390. [[CrossRef](#)]
8. Minami, T.; Sato, H.; Nanto, H.; Takata, S. Transparent conducting p-type NiO thin films prepared by magnetron sputtering. *Thin Solid Films* **1993**, *236*, 27–31.
9. Dong, Y.; Chen, Y.; Jiang, P.; Wang, G.; Wu, X.; Wu, R.; Zhang, C. Efficient and stable $\text{MoS}_2/\text{CdSe}/\text{NiO}$ photocathode for photoelectrochemical hydrogen generation from water. *Chem. Asian J.* **2015**, *10*, 1660–1667. [[CrossRef](#)] [[PubMed](#)]

10. Park, J.H.; Yoon, J.S.; Oh, S.Y. Characterization of a photoelectrochemical cell using porous TiO₂ and its application to a z-scheme system for water splitting in combination with a p-type InP photocathode. *J. Nanosci. Nanotechnol.* **2017**, *17*, 5593–5596. [[CrossRef](#)]
11. Li, Q.; Zheng, M.; Zhong, M.; Ma, L.; Wang, F.; Ma, L.; Shen, W. Engineering MoS_x/Ti/InP hybrid photocathode for improved solar hydrogen production. *Sci. Rep.* **2016**, *6*, 29738. [[CrossRef](#)] [[PubMed](#)]
12. Mckone, J.R.; Pieterick, A.P.; Gray, H.B.; Lewis, N.S. Hydrogen evolution from Pt/Ru-coated p-type WSe₂ photocathodes. *J. Am. Chem. Soc.* **2013**, *135*, 223–231. [[CrossRef](#)] [[PubMed](#)]
13. Shi, Z.W.; Lu, H.; Liu, Q.; Cao, F.R.; Guo, J.; Deng, K.M.; Li, L.A. Efficient p-type dye-sensitized solar cells with all-nano-electrodes: NiCo₂S₄ mesoporous nanosheet counter electrodes directly converted from NiCo₂O₄ photocathodes. *Nanoscale Res. Lett.* **2014**, *9*, 608–613. [[CrossRef](#)] [[PubMed](#)]
14. Jan, G.; Olga, P.; Roman, Y.; Kateřina, P. Hydrogen sensors based on electrophoretically deposited Pd nanoparticles onto InP. *Nanoscale Res. Lett.* **2011**, *6*, 392–396.
15. Gupta, N.; Sharma, C.; Kumar, M.; Kumar, R. Synthesis and comparative charge transfer studies in porphyrin—Fullerene dyads: Mode of attachment effect. *New J. Chem.* **2017**, *41*, 13276–13286. [[CrossRef](#)]
16. Joshi, U.A.; Maggard, P.A. CuNb₃O₈: A p-type semiconducting metal oxide photoelectrode. *J. Phys. Chem. Lett.* **2012**, *3*, 1577–1581. [[CrossRef](#)] [[PubMed](#)]
17. Nishikawa, M.; Fukuda, M.; Nakabayashi, Y.; Saito, N.; Ogawa, N.; Nakajima, T.; Shinoda, K.; Tsuchiya, T.; Nosaka, Y. A method to give chemical stabilities of photoelectrodes for water splitting: Compositing of a highly crystallized TiO₂ layer on a chemically unstable Cu₂O photocathode using laser-induced crystallization process. *Appl. Surf. Sci.* **2016**, *363*, 173–180. [[CrossRef](#)]
18. Liu, Y.; Wu, Y.; Zhang, W.; Zhang, J.; Wang, B.; Xia, C.; Afzal, M.; Li, J.; Singh, M.; Zhu, B. Natural CuFe₂O₄ mineral for solid oxide fuel cells. *Int. J. Hydrogen Energy* **2017**, *42*, 17514–17521. [[CrossRef](#)]
19. Chen, Y.; Mou, Z.; Yin, S.; Huang, H.; Yang, P.; Wang, X.; Du, Y. Graphene enhanced photocatalytic hydrogen evolution performance of dye-sensitized TiO₂ under visible light irradiation. *Mater. Lett.* **2013**, *107*, 31–34. [[CrossRef](#)]
20. Diez-Garcia, M.; Lana-Villarreal, T.; Gomez, R. Study of copper ferrite as a novel photocathode for water reduction: Improving its photoactivity by electrochemical pretreatment. *ChemSusChem* **2016**, *9*, 1504–1512. [[CrossRef](#)] [[PubMed](#)]
21. Hasselman, G.M.; Watson, D.F.; Stromberg, J.R.; Bocian, D.F.; Holten, D.; Lindsey, J.S.; Meyer, G.J. Theoretical solar-to-electrical energy-conversion efficiencies of perylene-porphyrin light-harvesting arrays. *J. Phys. Chem. B* **2006**, *110*, 25430–25440. [[CrossRef](#)] [[PubMed](#)]
22. Bian, Y.; Jiang, J. Recent advances in phthalocyanine-based functional molecular materials. In *50 Years of Structure and Bonding—The Anniversary Volume*; Springer: Heidelberg, Germany, 2015; Volume 172, pp. 159–199.
23. Hagiwara, H.; Higashi, K.; Watanabe, M.; Kakigi, R.; Ida, S.; Ishihara, T. Effect of porphyrin molecular structure on water splitting activity of a KTaO₃ Photocatalyst. *Catalysts* **2016**, *6*, 42. [[CrossRef](#)]
24. Roy, D.R.; Shah, E.V.; Roy, S.M. Optical activity of Co-porphyrin in the light of IR and Raman spectroscopy: A critical DFT investigation. *Spectrochim. Acta Part A* **2018**, *190*, 121–128. [[CrossRef](#)] [[PubMed](#)]
25. Wang, H.Y.A.; Song, T.; Sun, Q.; Liu, H.; Wang, T.; Zeng, H. Plasmon mediated Fe-O in octahedral site of cuprospinel by Cu NPs for photocatalytic hydrogen evolution. *Nanoscale* **2017**, *9*, 15760–15765. [[CrossRef](#)] [[PubMed](#)]
26. Nakhate, A.V.; Yadav, G.D. Solvothermal synthesis of CuFe₂O₄@rGO: Efficient catalyst for C-O cross coupling and N-arylation reaction under ligand-free condition. *ChemistrySelect* **2017**, *2*, 7150–7159. [[CrossRef](#)]
27. Wu, L.-K.; Wu, H.; Zhang, H.-B.; Cao, H.-Z.; Hou, G.-Y.; Tang, Y.-P.; Zheng, G.-Q. Graphene oxide/CuFe₂O₄ foam as an efficient absorbent for arsenic removal from water. *Chem. Eng. J.* **2018**, *334*, 1808–1819. [[CrossRef](#)]
28. Zhang, W.; Quan, B.; Lee, C.; Park, S.K.; Li, X.; Choi, E.; Diao, G.; Piao, Y. One-step facile solvothermal synthesis of copper ferrite-graphene composite as a high-performance supercapacitor material. *ACS Appl. Mater. Interfaces* **2015**, *7*, 2404–2414. [[CrossRef](#)] [[PubMed](#)]
29. Kang, Y.; Park, J.; Kim, D.-W.; Kim, H.; Kang, Y.-C. Controlling the antibacterial activity of CuSn thin films by varying the contents of Sn. *Appl. Surf. Sci.* **2016**, *389*, 1012–1016. [[CrossRef](#)]
30. Nayak, J.; Maniraj, M.; Gloskovskii, A.; Krajčí, M.; Sebastian, S.; Fisher, I.R.; Horn, K.; Barman, S.R. Bulk electronic structure of Zn-Mg-Y and Zn-Mg-Dy icosahedral quasicrystals. *Phys. Rev. B* **2015**, *91*. [[CrossRef](#)]

31. Min, S.; Lu, G. Sites for high efficient photocatalytic hydrogen evolution on a limited-layered MoS₂ cocatalyst confined on graphene sheets—the role of grapheme. *J. Phys. Chem. C* **2012**, *116*, 25415–25424. [[CrossRef](#)]
32. Jing, P.; Li, J.; Pan, L.; Wang, J.; Sun, X.; Liu, Q. Efficient photocatalytic degradation of acid fuchsin in aqueous solution using separate porous tetragonal-CuFe₂O₄ nanotubes. *J. Hazard. Mater.* **2015**, *284*, 163–170. [[CrossRef](#)] [[PubMed](#)]
33. Nawle, A.C.; Humbe, A.V.; Babrekar, M.K.; Deshmukh, S.S.; Jadhav, K.M. Deposition, characterization, magnetic and optical properties of Zn doped CuFe₂O₄ thin films. *J. Alloys Compd.* **2017**, *695*, 1573–1582. [[CrossRef](#)]
34. Zakeri, M.; Moghadam, M.; Mohammadpoor-Baltork, I.; Tangestaninejad, S.; Mirkhani, V.; Khosropour, A.R. Multi-wall carbon nanotube supported manganese(III) tetraphenylporphyrin: Efficient catalysts for epoxidation of alkenes with NaIO₄ under various reaction conditions. *J. Coord. Chem.* **2012**, *65*, 1144–1157. [[CrossRef](#)]
35. Kezzim, A.; Nasrallah, N.; Abdi, A.; Trari, M. Visible light induced hydrogen on the novel hetero-system CuFe₂O₄/TiO₂. *Energy Convers. Manag.* **2011**, *52*, 2800–2806. [[CrossRef](#)]
36. Chu, D.; Zhang, C.; Yang, P.; Du, Y.; Lu, C. WS₂ as an effective noble-metal free cocatalyst modified TiSi₂ for enhanced photocatalytic hydrogen evolution under visible light irradiation. *Catalysts* **2016**, *6*, 136. [[CrossRef](#)]
37. Xiao, P.; Guang, W.; Meng, W.; Liu, X.; Wen, S. Electrochemical synthesis of p-type Zn-doped α-Fe₂O₃ nanotube arrays for photoelectrochemical water splitting. *Chem. Commun.* **2013**, *44*, 5742–5744.
38. Wu, Y.; Yue, Z.; Liu, A.; Yang, P.; Zhu, M. P-type Cu-doped Zn_{0.3}Cd_{0.7}S/Graphene photocathode for efficient water splitting in a photoelectrochemical tandem cell. *ACS Sustain. Chem. Eng.* **2016**, *4*, 2569–2577. [[CrossRef](#)]
39. Chen, X.; Xia, N.; Yang, Z.; Gong, F.; Wei, Z.; Wang, D.; Tang, J.; Fang, X.; Fang, D.; Liao, L. Analysis of the influence and mechanism of sulfur passivation on the dark current of a single GaAs nanowire photodetector. *Nanotechnology* **2018**, *29*, 095201. [[CrossRef](#)] [[PubMed](#)]
40. Chen, Y.-H.; Wun, J.-M.; Wu, S.-L.; Chao, R.-L.; Huang, J.; Jan, Y.-H.; Chen, H.-S.; Chang, H.-S.; Ni, C.-J.; Chou, E.; et al. Top-illuminated In_{0.52}Al_{0.48}As-based avalanche photodiode with dual charge layers for high-speed and low dark current performances. *IEEE J. Sel. Top. Quant.* **2017**, *24*, 3800208. [[CrossRef](#)]
41. Zhao, Y.; Lin, C.; Bi, H.; Liu, Y.; Yan, Q. Magnetically separable CuFe₂O₄/AgBr composite photocatalysts: Preparation, characterization, photocatalytic activity and photocatalytic mechanism under visible light. *Appl. Surf. Sci.* **2017**, *392*, 701–707. [[CrossRef](#)]
42. Park, Y.; Kang, S.H.; Choi, W. Exfoliated and reorganized graphite oxide on titania nanoparticles as an auxiliary co-catalyst for photocatalytic solar conversion. *Phys. Chem. Chem. Phys.* **2011**, *13*, 9425–9431. [[CrossRef](#)] [[PubMed](#)]
43. Krol, R.V.D.; Liang, Y.; Schoonman, J. Solar hydrogen production with nanostructured metal oxides. *J. Mater. Chem.* **2008**, *18*, 2311–2320. [[CrossRef](#)]
44. Walter, M.G.; Warren, E.L.; Mckone, J.R.; Boettcher, S.W.; Mi, Q.X.; Santori, E.A.; Lewis, N.S. Solar water splitting cells. *Chem. Rev.* **2010**, *110*, 6446–6473. [[CrossRef](#)] [[PubMed](#)]
45. Hisatomi, T.; Kubota, J.; Domen, K. Recent advances in semiconductors for photocatalytic and photoelectrochemical water splitting. *Chem. Soc. Rev.* **2014**, *43*, 7520–7535. [[CrossRef](#)] [[PubMed](#)]

